Scaling dependence and synchronization of forced mercury beating heart systems

Animesh Biswas, Dibyendu Das, and P. Parmananda
Department of Physics, Indian Institute of Technology Bombay, Powai, Mumbai 400 076, India
(Received 5 December 2016; published 10 April 2017)

We perform experiments on a nonautonomous Mercury beating heart system, which is forced to pulsate using an external square wave potential. At suitable frequencies and volumes, the drop exhibits pulsation with polygonal shapes having n corners. We find the scaling dependence of the forcing frequency ν_n on the volume V of the drop and establish the relationship $\nu_n \propto \frac{n}{\sqrt{V}}$. It is shown that the geometrical shape of substrate is important for obtaining closer match to these scaling relationships. Furthermore, we study synchronization of two *nonidentical* drops driven by the same frequency and establish that synchrony happens when the relationship $n_2/n_1 = \sqrt{V_2/V_1}$ is satisfied.

DOI: 10.1103/PhysRevE.95.042202

I. INTRODUCTION

Liquid of a spherical drop or a circular column in shape undergoes dynamical motion like vibration due to the surface tension and inertia with or without external forces. For the dynamical properties of liquid, various attempts have been made to determine the eigenmodes and eigenfrequencies of oscillations. According to Rayleigh [1], the theoretically predicted resonance frequency for oscillating liquid drop (spherical in shape) is

$$\nu_n = \left[\frac{n(n-1)(n+2)\gamma}{3\pi\rho V}\right]^{1/2}, \tag{1}$$

where ν_n is the frequency of the nth eigenstate of the oscillations, ρ is the density, V is volume, and γ is the surface tension of the liquid drop. Rayleigh developed his theory on oscillating water jets. Oscillations can be observed in various natural, chemical, mechanical, electrical, biological, and electrochemical systems. Mercury beating heart (MBH) is one such electrochemical system, where oscillations of a mercury drop occur. In this work, we are interested in studying the MBH system and testing if any part of the Rayleigh's equation [Eq. (1)] is relevant to the dynamics of the oscillating drop.

A. MBH system

Oscillations in an electrochemical system [2–5] can occur when the system is far from the equilibrium. An MBH system is one such system which shows chemomechanical oscillations of the mercury drop. The mechanical oscillations (due to the imbalance of surface tension forces and electrostatic charges) of the mercury drop occur around the equilibrium point of oscillations. The electrochemical oscillations which drive the mechanical oscillations (by periodic charging and discharging) occur far from equilibrium. The system requires a mercury drop placed in a concave vessel and covered with an aqueous acidic or basic solution. Due to the interactions between water molecules, electrolyte ions, and mercury surface, an electric double layer is formed which is related to the distribution of electric charges over the mercury drop surface. In the presence of the strong oxidant in an acidic solution, an iron nail is used to trigger the oscillations of the mercury drop, where the charge distribution and surface energy of the drop change. Oscillations of the mercury drop in the MBH system can be visually observed, and, if performed carefully, the experimental results are fairly reproducible.

The original MBH system, observed by Kühne, was subsequently reported experimentally by Lippmann [6], who proposed the electrocapillarity effect as the cause of the oscillations of the mercury drop. The dynamical behavior entails electrochemical reactions coupled with the hydrodynamic motion of the mercury. However, the detailed mechanism of the oscillations in the MBH system was not well established in this work.

Joel *et al.* [7] analyzed the reactions and mechanisms of the MBH system with the mercury in a glass tube configuration and covering it with both acidic and basic solutions. It was realized that the formation and removal of the surface film (e.g., Hg_2SO_4) is the key element for the oscillations of the mercury drop. Oscillations depend on the nail position and on the chemical composition of the solution.

Smolin and Imbihl [8] carried out the study of MBH hydrodynamics modes in linear ring-shaped geometries varying the potential of the metal tip connected to the mercury drop. Olson *et al.* [9] described the oscillations in the MBH system, replacing the chemical driving force in the system (studied by Joel *et al.* [7]) by a power supply (voltage pulse). They conducted the experiments in a three-electrode MBH system where the external potential was controlled by a potentiostat and found concentric circles of different modes (lobe numbers or oscillations shape) of the oscillating mercury drop. In the work of Castillo-Rojas *et al.* [10], they found different modes of oscillation, such as a circle, pentagon, hexagon, and 8- and 16-fold stars in a watch glass geometry using the γ irradiation to generate the species Hg_2^{2+}.

Dinesh *et al.* [11] introduced the nonautonomous dynamics of the MBH system, which is different from the previous experiments. The system was forced periodically with a square wave potential in the absence of any oxidizing agent while the mercury drop is covered with an acidic solution (H_2SO_4). They observed various shapes (elliptical, triangular, pentagonal, hexagonal, and multilobed star shapes) of the oscillating mercury drop as a function of frequency of the applied potential and found a linear relation between the lobe number n and frequency ν_n, $n \propto \nu_n$. Subsequently, the MBH systems dynamics have been studied experimentally [12–15] under different conditions.

B. Synchronization

The coupling of two or more oscillators shows interesting behavior of nonlinear systems like synchronization. Synchronization is the adjustment of the rhythms of oscillators due to the interactions between them [16–18]. Synchronization can also occur in an ensemble of oscillators and is usually studied in self-sustained, periodic, and chaotic systems (oscillators).

Synchronization among the oscillators could be weak, intermediate, or strong and is analyzed using the time evolution of the observables recorded from the interacting oscillators. Synchronization phenomena have been classified mainly into four types, no synchronization, phase synchronization, lag synchronization, and complete synchronization [19,20]. In no synchronization, the oscillations of coupled oscillators do not show any correlation in the phases or in the amplitudes of the time series of the coupled systems. In phase synchronization, the temporal variation of their phases remains same, but their amplitudes vary. Oscillators could have a constant phase difference, but the same amplitudes at the comparatively high coupling strength, and that is defined as lag synchronization. Finally, the complete synchronization can be observed wherein the activities of the coupled oscillators have identical phases and amplitudes.

Synchronization depends on the coupling strength and the way the oscillators are coupled. The information can flow in one direction or in both directions between coupled oscillators. In unidirectional coupling, information transfer occurs in one direction where the first oscillator influences the second oscillator only and remains unaffected by the second one. In bidirectional coupling, information flows in both directions between the two oscillators. In another kind of synchronization, the oscillators are driven by a common forcing frequency. Synchronization in various autonomous (physical, chemical, mechanical) systems is a well-studied phenomena in diverse fields. Synchronization of MBH systems has previously been reported by Dinesh *et al.* [21,22].

C. Outline of Results

In the present work, we examine the dynamics of the nonautonomous MBH system introduced by Dinesh *et al.* [11]. Two sets of experiments are performed. In the first part we try to understand the scaling dependence of frequency ν_n of the external applied potential on volume V and then on lobe number n. Rayleigh's equation [Eq. (1)] suggests that $\nu_n \propto \frac{1}{\sqrt{V}}$ and Dinesh *et al.* [11] work found that $n \propto \nu_n$. We checked the combined validity of the two relations in the forced MBH system:

$$\nu_n \propto \frac{n}{\sqrt{V}}. \tag{2}$$

In the second part, the synchronization of two nonidentical nonautonomous MBH oscillators (different volumes and lobe numbers) was studied. The goal here is to synchronize two nonautonomous MBH oscillators by applying the same forcing potential even when they are exhibiting different lobe numbers of oscillations. It is observed that, when the MBH systems are synchronized, the lobe numbers (n_1,n_2) and volumes (V_1,V_2) follow Eq. (3) as given below. We note that our system has bidirectional coupling and shows phase synchronization.

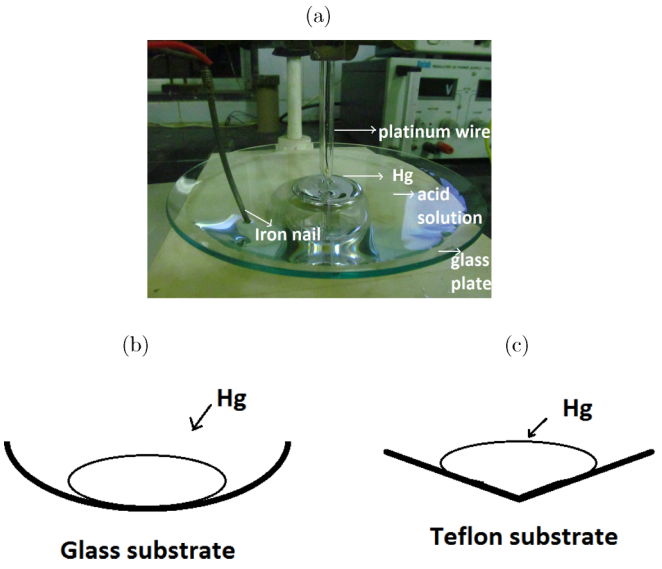

FIG. 1. (a) A view of the experimental setup showing the glass plate, mercury drop and the electrodes. (b) The curved glass substrate. (c) The conical Teflon substrate with a linear radial profile.

II. SINGLE-DROP OSCILLATION: EXPERIMENTAL SETUP AND UNDERLYING CHEMICAL REACTIONS

In order to test the relation in Eq. (2) we study the various lobe numbers of oscillations (n) of a single mercury drop for different volumes (V) and external voltage frequencies (ν_n) on two different substrates (glass and Teflon).

A mercury drop is placed on a glass or Teflon substrate of diameter of 15 cm. The drop is covered by 1 M H_2SO_4 acidic solution. The system is driven by an external oscillatory voltage of a square waveform; this is applied through the contact of the exposed tip of a platinum wire covered with parafilm with the mercury drop. This small tip is placed such that it touches only the center position of the mercury drop and not the acidic solution. One iron nail is placed vertically into the acidic solution and far from the mercury drop (i.e., not touching it even as it oscillates), serving as an electrode. To provide square wave potential, we used a function generator (Tektronix, AF 3021B) with 10 V_{pp} magnitude. Various parts of the experimental setup are shown in Fig. 1(a). The two substrates, the glass and Teflon, are used and are schematically shown in Figs. 1(b) and 1(c), respectively. The distinction of the conical surface of Teflon [Fig. 1(c)] as compared to glass [Fig. 1(b)] is that the angle of tangent to the surface is the same at all contact points between the substrate and the drop, and this helps in getting cleaner results for the system using Teflon.

Let us briefly discuss the redox reactions involved in the MBH process. In the nonautonomous MBH system, in the presence of the applied external potential between the mercury drop and iron electrodes and dissolved O_2, oxidation and reduction processes occur cyclically. Due to oxidation, charges accumulate on the drop surface and increase its area, simultaneously flattening it. This charging is followed by a discharging process, associated with a reduction reaction during which the drop contracts back to its initial shape. The competition between the forces of surface tension and

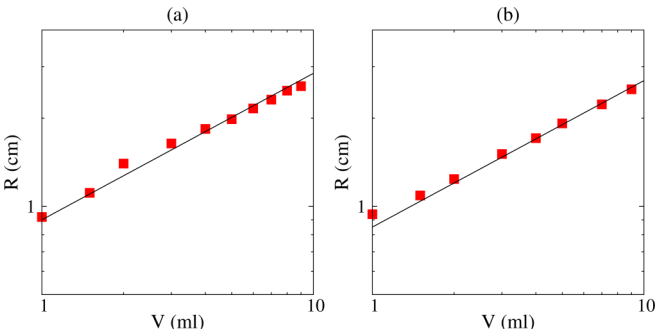

FIG. 2. Logarithmic plot of observed radius R of the mercury drop vs the drop volume V on (a) the glass plate and (b) the Teflon plate. Solid lines show power law fits to both the figures with power 0.5.

electrostatic charges during the charging and discharging of the drop leads to mechanical oscillations of the drop. The reactions are as follows:

a. The oxidation cycle:

At anode (Hg): $2Hg^0 \longrightarrow Hg_2^{2+} + 2e^-$

At cathode (Fe): $O_2 + 2H^+ + 2e^- \longrightarrow H_2O$

Hg_2^{2+} is the free ion in the solution, and it combines with the sulfate ion $[SO_4^{2-}(aq)]$ to form the insoluble Hg_2SO_4 film on the mercury surface:

$Hg_2^{2+} + SO_4^{2-}(aq) \rightleftharpoons Hg_2SO_4$ (insoluble)

b. Reduction cycle:

At anode (Fe): $Fe \longrightarrow Fe^{2+} + 2e^-$

At cathode (Hg drop): $Hg_2^{2+} + 2e^- \longrightarrow 2Hg^0$

The above redox reactions lead to oscillations of the mercury drop which continue until all H^+ ions are converted to H_2O.

The shape of mercury drop is not spherical as it flattens under gravity on the substrate (glass or Teflon plate). Rayleigh considers spherical drop in his work, so the volume $V \propto R^3$ in Eq. (1), where R is the radius of the undisturbed drop. In this work, the mercury drop is roughly cylindrical in shape so that volume $V \propto R^2$. Experimental evidence for this is presented in Fig. 2 for both the glass and teflon plates. The images of the drops were taken from the top. The radii of the drops were calculated using an image-processing method in Matlab.

It was shown in Dinesh *et al.* [11] that in a nonautonomous MBH system various polygonal pulsating drops are produced as a function of frequency of the applied voltage for a fixed volume. Here for completeness, four such shapes are shown in Fig. 3. Depending on the number of sharp corners, each shape is labeled by a lobe number n. In the Figs. 3(a)–3(d) drops with $n = 2$, 3, 5, and 6 are shown. Next it is shown that the lobe numbers vary with the simultaneous variation of the external voltage frequency as well as the drop volume.

Results

In Dinesh *et al.* [11] it was shown that the lobe numbers of the pulsating drop increases *linearly* with the frequency of the applied voltage. Note that this is different from the expression of Rayleigh [1] [Eq. (1)]. In the present work, the simultaneous dependence of lobe number on volume and frequency is examined. The volume of the mercury drop was varied within

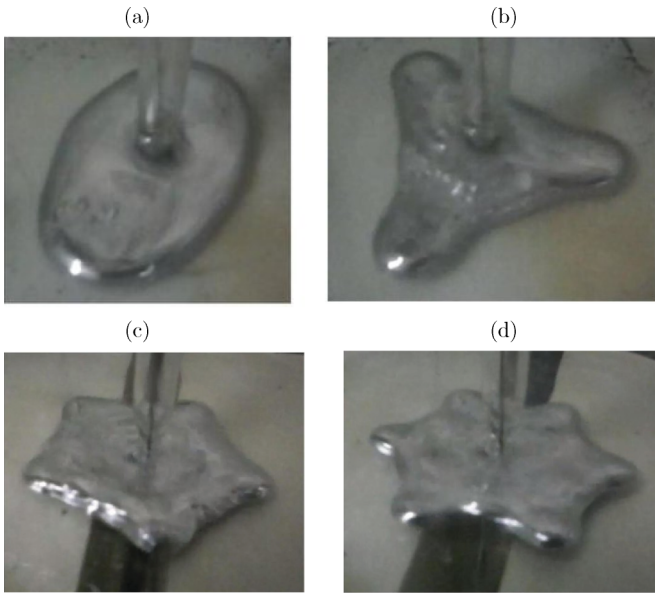

FIG. 3. Shapes of oscillating mercury drops: (a) elliptical ($n = 2$), (b) triangular ($n = 3$), (c) pentagonal ($n = 5$), (d) hexagonal ($n = 6$).

the range 1–10 ml in steps of 1 ml. Subsequently, the frequency of the applied voltage was changed slowly in steps of 0.2 Hz. We waited to see that for a chosen volume of the drop V, external frequency ν_n stabilized a pulsation of lobe number n. For three such n values a logarithmic plot of the frequency ν_n against volume V was plotted (Fig. 4). Reasonable power law dependences $\sim V^{-0.5}$ are seen, the data for Teflon being closer to the theoretical fit compared to the glass substrate. Furthermore, the simultaneous dependence is presented by plotting the scaled variable ν_n/n against V in Fig. 5. Data collapse is seen, confirming the power law expectation from Eq. (1). Thus the volume dependence of ν_n is indeed like in Rayleigh [1], although the lobe number dependence is distinct.

III. SYNCHRONIZATION OF TWO COUPLED NONIDENTICAL MBH OSCILLATORS

Synchronization of multiple coupled but identical autonomous MBH oscillators (i.e., drops of equal volume,

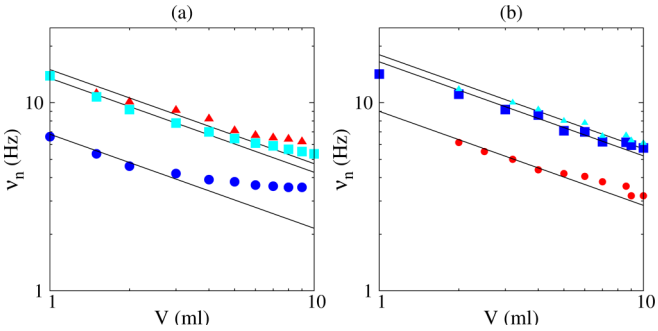

FIG. 4. Logarithmic plot of frequency ν_n vs mercury drop volume V for $n = 3$ (●), 5 (■), 6 (▲), for (a) the glass plate and (b) the Teflon plate. Solid lines show the power law fits with power −0.5.

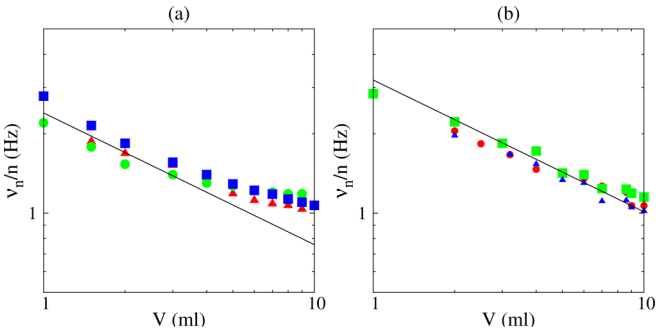

FIG. 5. Logarithmic plot of frequency or lobe number (ν_n/n) vs mercury drop volume V for $n = 3$ (●), 5 (■), 6 (▲), for (a) the glass plate and (b) the Teflon plate. Solid line shows the power law fits with power −0.5.

pulsating with same lobe number) have been studied [21,22]. Here the goal is to explore the possibility of synchronization of two nonidentical oscillators (i.e., drops of different volume, pulsating with different lobe numbers). The two MBH oscillators are forced with the same forcing potential (same frequency and amplitude) from the two different function generators prior to the coupling and subsequently coupled through a variable resistance box, where the drop volume of the one oscillator is kept fixed, while the other is varied. It is found that for certain specific values of the volume of the second oscillator, nonidentical pulsating lobe numbers of the two oscillators synchronize.

The experimental setup (schematic presented in Fig. 6) of two coupled MBH oscillators is shown in Fig. 7. The substrate, reagents, electrodes, and external potential are identical to the single-drop system described in the previous section. The new thing is the bidirectional coupling via a resistance box. The coupling resistance is kept very low (15–70 Ω) to ensure that the coupling is strong.

In the experiment, to begin, the frequencies of external driving potential of the two oscillators are set to be equal to a certain value. For example, the results in the next subsection are presented for $\nu^{(1)} = \nu^{(2)} = 7.3$ Hz (superscripts stand for oscillator numbers 1 and 2). Then the volume V_1 of the first drop is adjusted so that it pulsates at a certain lobe number n_1 of our choice. From Eq. (2) it would be expected that $\nu^{(1)}_{n_1} \propto n_1/\sqrt{V_1}$. Then the volume V_2 of the second drop is varied incrementally in a small steps of 0.1 ml. We wanted to see if a volume V_2, at which a certain pulsating lobe of lobe number n_2 stabilizes for the second drop *in synchrony with the*

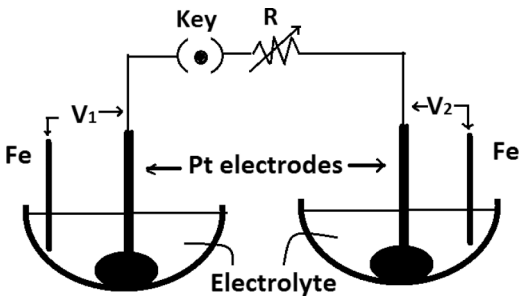

FIG. 6. Schematic diagram for the bidirectional coupling.

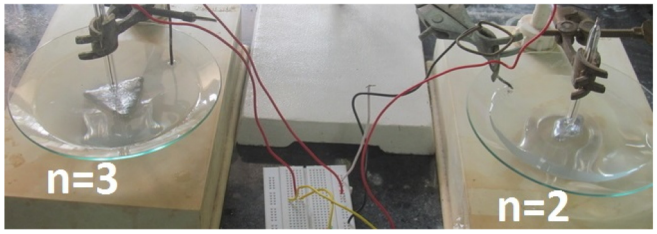

FIG. 7. View of the experimental setup with two coupled nonidentical oscillators. Different shapes of the drops, triangular ($n_1 = 3$) and elliptical ($n_2 = 2$), may be seen.

pulsation of the first drop satisfies the desired relationship:

$$\left(\frac{V_2}{V_1}\right)^{1/2} = \frac{n_2}{n_1}. \tag{3}$$

This is a reasonable expectation given that in isolation the second drop has $\nu^{(2)}_{n_2} \propto n_2/\sqrt{V_2}$, and as the frequency is set to $\nu^{(2)} = \nu^{(1)}$. Yet it is interesting to note that synchronization of the two drops in nonidentical conditions is being tested. The experimental observations are presented below, and to characterize the extent of synchrony a suitable quantitative measure is defined and used. It will be seen that as V_2 is increased, higher lobe numbers (n_2) appear on the second drop, and for specific rational numbers (n_2/n_1) where Eq. (3) is satisfied, enhanced synchrony is observed.

Results

Experimentally, the oscillation of the two drops are characterized by the time-dependent distance D of a polygonal corner from the center of the drop. Videos of the oscillating drops are recorded, and images are extracted from the videos using online software (Free Video to JPG converter v. 5.0.63 build 913). The values of D of the two drops are plotted as a function of camera frame number in Fig. 8. The intervals between the frame numbers are 0.033 s. As stated above $\nu^{(1)} = \nu^{(2)} = 7.3$ Hz was used. $n_1 = 5$ was set by choosing $V_1 = 3.6$ ml. Then the volume V_2 is varied over the range 0.1–10 ml in steps of 0.1 ml. In Figs. 8(a)–8(i) the first lobe shows regular oscillation of the distance D corresponding to its lobe number $n_1 = 5$. In contrast, the lobes of the second oscillating drop show the oscillations in the distance D with a concentric circular mode [Figs. 8(a), 8(e), and 8(f)], irregular mixed lobe numbers [Figs. 8(c) and 8(h)], and with well-defined lobe numbers n_2 in synchrony with the first drop [Figs. 8(b), 8(d), 8(g), and 8(i)]. It can be observed the synchrony appears, disappears, and reappears as V_2 is varied.

To quantify the synchronization behavior, cross-correlation coefficient (CCC) is measured between the oscillations of the two distances $D^{(1)}_j$ and $D^{(2)}_j$ at every frame number j defined as follows:

$$CCC = \frac{\sum_j \left(D^{(1)}_j - \bar{D}^{(1)}\right)\left(D^{(2)}_j - \bar{D}^{(2)}\right)}{\sqrt{\sum_j \left(D^{(1)}_j - \bar{D}^{(1)}\right)^2 \left(D^{(2)}_j - \bar{D}^{(2)}\right)^2}}, \tag{4}$$

where $\bar{D}^{(1)}$ and $\bar{D}^{(1)}$ are the averages of $D^{(1)}_j$ and $D^{(2)}_j$ respectively.

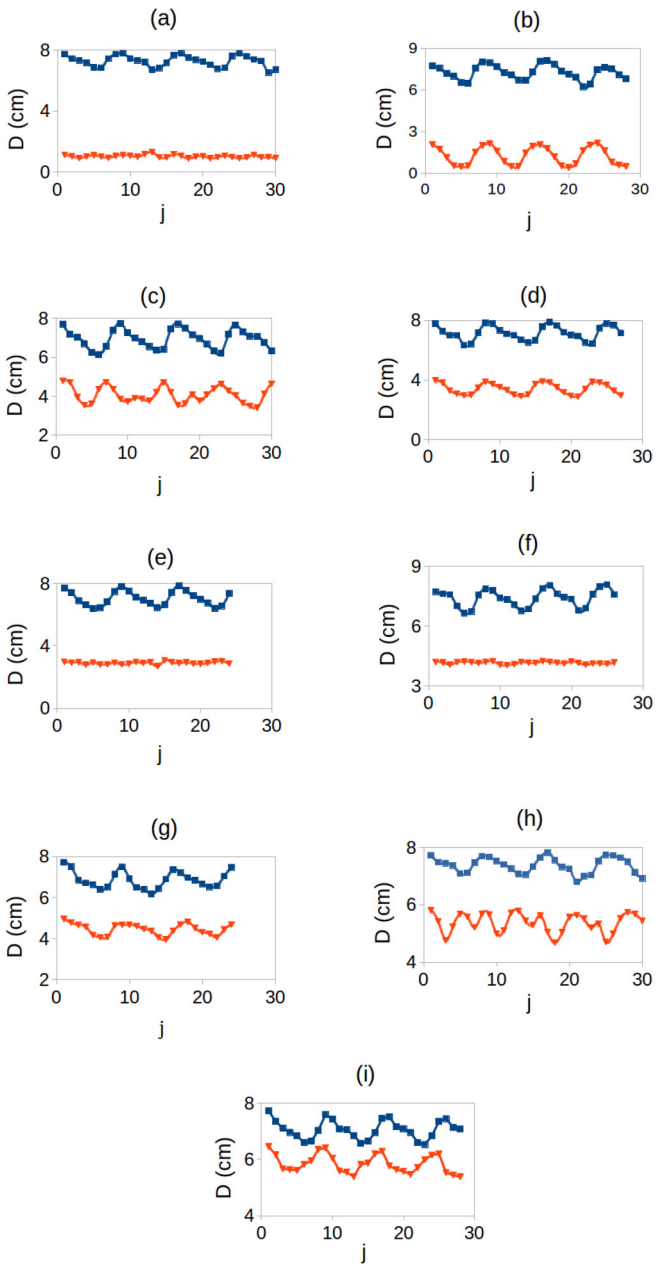

FIG. 8. Radial distance D of the two mercury drops on glass plates, plotted as a function of the frame number j (equivalent to time series). The nine subfigures (a)–(i) correspond to the different points indicated in the curves in Fig. 9. Applied frequencies are $\nu_1 = \nu_2 = 7.3$ Hz and $V_1 = 3.6$ ml. The signals $D^{(1)}$, $D^{(2)}$ for the first and the second drops in all subfigures are denoted by ■ and ▼, respectively. The different subfigures correspond to the following pairs of lobe numbers: (a) $n_1 = 5, n_2 = 0$ (circular), (b) $n_1 = 5, n_2 = 2$, (c) $n_1 = 5, n_2 =$ mixed lobe numbers, (d) $n_1 = 5, n_2 = 3$, (e) $n_1 = 5, n_2 = 0$ (circular), (f) $n_1 = 5, n_2 = 0$ (circular), (g) $n_1 = 5, n_2 = 5$, (h) $n_1 = 5, n_2 =$ mixed lobe number, (i) $n_1) = 5, n_2 = 6$.

CCC is plotted as a function of $\sqrt{V_2/V_1}$ in Figs. 9(a)–9(b). Corresponding to Fig. 8(a) the CCC value is found very low in Fig. 9(a). Corresponding to Fig. 8(b), the CCC is found to a value to peak, but the $\sqrt{V_2/V_1}$ value is slightly less (≈0.3) than the ratio $n_2/n_1 = 2/5$ as expected from Eq. (3). Having

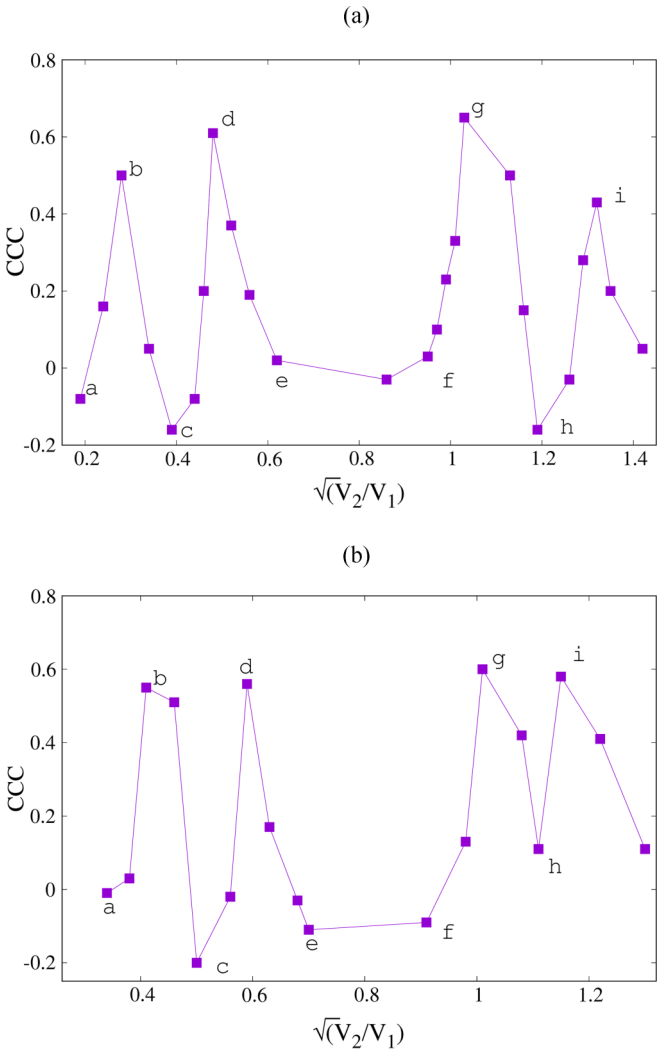

FIG. 9. CCC vs $\sqrt{V_2/V_1}$ for (a) $n_1 = 5$, $V_1 = 3.6$ ml, $\nu_1 = \nu_2 = 7.3$ Hz, on a glass substrate, and (b) $n_1 = 5$, $V_1 = 3$ ml, $\nu_1 = \nu_2 = 8.2$ Hz, on a Teflon substrate.

performed a similar experiment with the Teflon substrate it is found [Fig. 9(b)] that the corresponding peak is at $\sqrt{V_2/V_1} \approx 0.4$; thus Eq. (3) works almost perfectly. This is followed by a dip in CCC corresponding to Fig. 8(c). The next peak appears at $\sqrt{V_2/V_1} \approx 0.5$ for the glass substrate [Fig. 9(a)], which is again slightly less than the expected ratio $n_2/n_1 = 3/5$ from Eq. (3), while for the Teflon geometry the peak position is almost at $\sqrt{V_2/V_1} \approx 0.6$ [see Fig. 9(b)]. It should be noted that we never found a stable oscillatory shape of lobe number $n_2 = 4$, so there is no peak at $\sqrt{V_2/V_1} = 4/5$. Again a dip is seen corresponding to Fig. 8(e) and then the next peak at $\sqrt{V_2/V_1} \approx 1.0$ for the glass as well as the Teflon substrate and which is the same as $n_2/n_1 = 5/5 = 1$ (the case of synchrony of identical oscillators). Finally, again the CCC plunges corresponding to Fig. 8(h). The next peak [Fig. 8(i)] expected according to Eq. (3) at $\sqrt{V_2/V_1} = n_2/n_1 = 6/5$ is seen at values ≈1.3 and ≈1.2 for the glass and Teflon substrates, respectively.

Figure 9 describes a single experimental run obtained by incrementally increasing the volume V_2 of the second drop. Many such experimental runs were performed, and the peaks

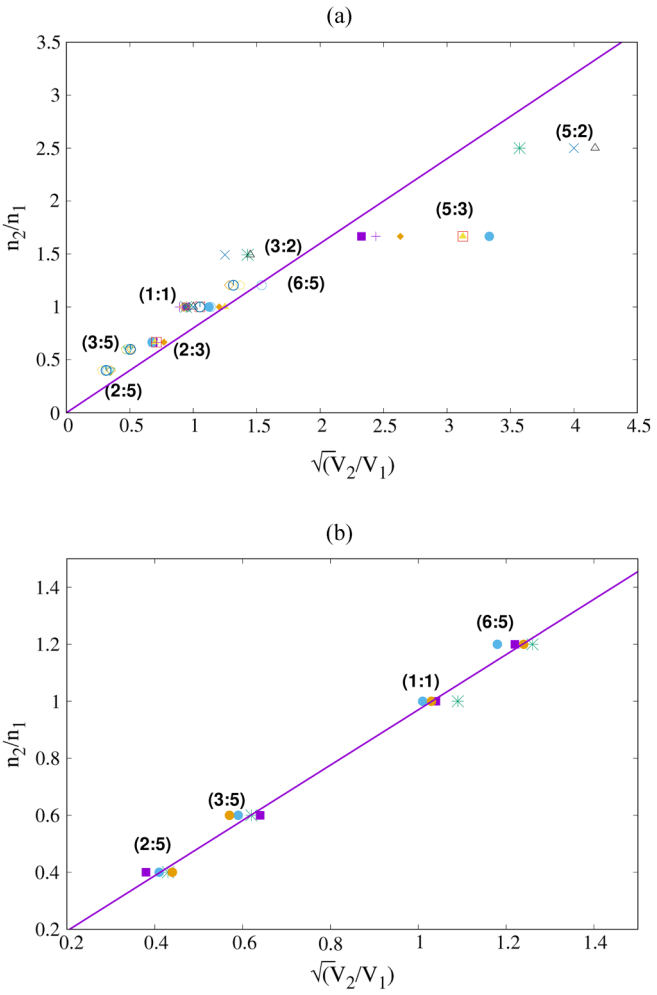

FIG. 10. Plot of lobe number ratios (n_2/n_1) of the oscillating drops of the two oscillators vs $\sqrt{V_1/V_2}$ on (a) a glass substrate and (b) a Teflon substrate. The solid lines correspond to straight lines with unit slopes.

in CCC obtained at various values of $\sqrt{V_2/V_1}$ along with their corresponding lobe numbers ratios n_2/n_1 gave us a data set. All the points in this data set are plotted against a straight line with unit slope [reflecting Eq. (3)] as shown in Figs. 10(a) and 10(b) for the glass and Teflon substrates, respectively. For Teflon, the match is nearly perfect, while for glass it is close.

IV. CONCLUSIONS

Two sets of experiments were performed on MBH systems, where an electrochemical redox reaction produces pulsating drops with polygonal shapes. The driving frequency ν_n, lobe number n, and volume V of such a drop has interesting power law relationships among themselves. A dependence of $n \propto \nu_n$ was known from an earlier experiment [11]. The first goal of the present paper was to explore the scaling relationship of frequency (ν_n) to volume (V). In this regard, it was verified for a single-drop oscillation, $\nu_n \propto 1/\sqrt{V}$ [Eq. (2)] similar to the prediction of Rayleigh [Eq. (1)]. In the second set of experiments, the synchrony of two coupled nonidentical mercury drop systems driven at the same frequency was demonstrated. It was found that precisely close to where the relationship $\sqrt{V} \propto n$ [see Eq. (3)] is satisfied for both the drops, there is an enhancement (peak) of cross-correlation coefficient (CCC), implying enhanced synchronous activity (Fig. 9). Thus synchronization follows the scaling relation in Eq. 3 (Fig. 10). Moreover, the effect of substrate geometry [Figs. 1(b)–1(c)] on the algebraic dependence on volume was also studied. In Figs. 5, 9, and 10, we compared the results for a curved glass substrate to a Teflon substrate with a linear shape in the radially outward direction. It was found that the experiments on the Teflon substrate give much better convergence to the scaling relationship on volume. This could be because the Teflon surface provides same tangential contact direction to drops of different sizes and thus ensures some uniformity, as compared to the curved glass surface. At least, experimentally, this uniformity seems to matter in producing cleaner scaling results.

Real systems are not exactly identical due to the inherent parameter mismatches in the systems. So it is important and interesting to study the synchronization between the nonidentical systems. In this work, we came up with an approach to achieve the synchonization behavior between two nonidentical nonautonomous MBH oscillators. As Figs. 8 and 9 indicate, a coupled state of two MBH oscillators with different stable oscillating lobe numbers of the mercury drops and different drop volumes can indeed be synchronized. To the best of our knowledge this is the first time the study of synchrony has been done on a forced chemical system. Furthermore, the synchronization of two nonidentical systems exhibiting different dynamical behavior is indeed challenging and a novel problem. This is precisely due to the fact that coupling is seldom able to dominate the forcing term. In our experiment, we were able to exploit the scaling relation to devise the situation where coupling could indeed overcome the forcing term and consequently two nonidentical forced systems could attain synchronization.

ACKNOWLEDGMENTS

The authors acknowledge financial support from IIT Bombay and DST India (project reference no. EMR/2016/000275). We also thank members of our Nonlinear Dynamics Laboratory group for constructive discussions.

[1] Lord Rayleigh, Proc. R. Soc. Lond. **29**, 71 (1879).
[2] H. D. Dewald, P. Parmananda, and R. W. Rollins, J. Electroanal. Chem. **306**, 297 (1991).
[3] H. D. Dewald, P. Parmananda, and R. W. Rollins, J. Electrochem. Soc. **140**, 1969 (1993).
[4] C. Zensen, K. Schönleber, F. Kemeth, and K. Krischer, J. Phys. Chem. C **118**, 24407 (2014).
[5] V. García-Morales and K. Krischer, Phys. Rev. E **78**, 057201 (2008).
[6] G. Lippman, G. Ann. Phys. (Berlin), **149**, 565 (1873).

[7] J. Keizer, P. A. Rock, and S. W. Lin, J. Am. Chem. Soc. **101**, 5637 (1979).
[8] S. Smolin and R. Imbihl, J. Phys. Chem. **100**, 19055 (1996).
[9] J. Olson, C. Ursenbach, V. I. Birss, and W. G. Laidlaw, J. Phys. Chem. **93**, 8258 (1989).
[10] S. Castillo-Rojas, J. González-Chávez, L. Vicente, and G. Burillo, J. Phys. Chem. A **105**, 8038 (2001).
[11] D. K. Verma, A. Q. Contractor, and P. Parmananda, J. Phys. Chem. A **117**, 267 (2013).
[12] D. Anvir, J. Chem. Educ. **66**, 211 (1989).
[13] C. W. Kim, I. H. Yeo, and W. K. Paik, Electrochem. Acta **41**, 2829 (1996).
[14] E. Ramírez-Álvarez, J. L. Ocampo-Espindola, F. Montoya, F. Yousif, F. Vízquez, and M. Rivera, J. Phys. Chem. A **118**, 10673 (2014).
[15] J. L. Ocampo-Espindola, E. Ramírez-Álvarez, F. Montoya, P. Parmananda, and M. Rivera, J. Solid State Electrochem. **19**, 3297 (2015).
[16] S. H. Strogatz and I. Stewart, Sci. Am. **269**, 102 (1993).
[17] S. Boccaletti, J. Kurths, G. Osipov, D. L. Valladares, and C. S. Zhou, Phys. Rep. **366**, 1 (2002).
[18] F. E. Hanson, Fed. Proc. **37**, 2158 (1978).
[19] M. Rivera, G. Martnez Mekler, and P. Parmananda, Chaos **16**, 037105 (2006).
[20] J. M. Cruz, M. Rivera, and P. Parmananda, Phys. Rev. E **75**, 035201 (2007).
[21] D. K. Verma, H. Singh, A. Q. Contractor, and P. Parmananda, J. Phys. Chem. A **118**, 4647 (2014).
[22] D. K. Verma, H. Singh, P. Parmananda, A. Q. Contractor, and M. Rivera, Chaos **25**, 064609 (2015).